Solid Freeform Fabrication Symposium, Austin, TX, Aug. 12-14, 2013.

Reverse Engineering of Materials using Surfacelet-based Methods for CAD-Material Integration

Namin Jeong, David W. Rosen
The George W. Woodruff School of Mechanical Engineering
Georgia Institute of Technology
Atlanta, GA 30332-0405

To integrate material information into CAD systems, geometric features of material microstructure must be recognized and represented, which is the focus of this paper. Linear microstructure features, such as fibers or grain boundaries, can be found computationally from microstructure images using surfacelet based methods, which include the Radon or Radon-like transform followed by a wavelet transform. By finding peaks in the transform results, linear features can be recognized and characterized by length, orientation, and position. The challenge is that often a feature will be imprecisely represented in the transformed parameter space. In this paper, we demonstrate surfacelet-based methods to recognize microstructure features in parts fabricated by additive manufacturing. We will provide an explicit mathematical method to recognize and to quantify linear geometric features from an image.

1 INTRODUCTION

For many years, practitioners in the additive manufacturing (AM) industry have cited the lack of suitable engineering materials as a major challenge. Others note the large variability and unpredictability of mechanical properties in AM processed materials. Both sets of users would benefit from computer-aided design (CAD) tools that integrate material information with geometry. Furthermore, the capability of deriving mechanical properties from the material and geometry information would greatly aid part design and engineering [1]. Models of material composition and geometry are integrated in what is called heterogeneous CAD modeling. Integration of material composition, microstructure, and mechanical properties with geometry information enables many product development activities, including design, analysis, and manufacturing. However, typical approaches utilize continuous distributions of material compositions modeled parametrically using volume fraction methods. This approach is only focused on macro-scale part models, while microstructure of the models is not considered. Furthermore, such material composition models only represent the designer's desire or specification, but the physical behavior of the actual materials is not recognized. Also, the actual material composition may deviate from the specification due to the specifics of manufacturing processes, heat treatments, or other material limitations. In this paper, we investigate the application of image processing methods for constructing models of material microstructure. With these microstructure models, heterogeneous CAD systems will be enabled.

In order to support the CAD system mentioned above, geometric features of material microstructure have to be recognized and represented, which is the focus of this paper. In recognition of the need of microscopic materials modeling for heterogeneous CAD systems, we

present a new method for reverse engineering of composite materials such that models of material microstructure can be constructed and used as CAD representations to support heterogeneous part modeling. Such material models capture microscopic features and enable integration with structure-property relationships.

In recognition of the need of microscopic materials modeling for heterogeneous CAD systems, we present a new method for reverse engineering of materials such that microstructure models can be constructed and used as CAD representations to support heterogeneous part modeling. A new method for reverse engineering of materials is shown schematically in Figure 1 .

A material sample is sliced and imaged at appropriate resolutions to capture the geometric features of its microstructure. This is defined as the structure, represented by lines, angles, curves, and shapes, which are related to each other, of the prepared surface of a material sample at the microscopic level. Capturing these geometric features from a microstructure image enables structure-property relationships to be constructed at the desired level of scale. Before image analysis, the user specifies material compositions (i.e., which colors or shades correspond to which materials). Image analysis is performed to extract the geometry of material's microstructure (e.g., grain or particle size, shape, orientation) and to correlate it with material compositions. In order to obtain structure-property relationships, the extracted geometry features are integrated into CAD systems. By constructing a microstructure model, the effective mechanical properties (e.g., Poisson's ratio, elastic modulus etc.) can be calculated. Therefore, structure-property relationships are established. As a result, we will have the ability to construct heterogeneous models of materials that can be integrated into CAD system and used for mechanical part design.

In this paper, we will focus on the recognition of linear features of the microstructure of material using proposed method. Linear microstructure features, such as fibers or grain boundaries, can be found computationally using surfacelet methods, which includes the Radon or Radon-like transform followed by wavelets transform. By analyzing the results, linear features can be recognized and characterized by length, orientation, and position. In the remainder of the paper, in section 2, background of heterogeneous modeling and feature extraction on microstructure are introduced. In Section 3, we introduce a new method for recognizing geometric features. Furthermore, the result of feature extraction and its discussion will be followed in section 4. Lastly, conclusion will be given in section 5.

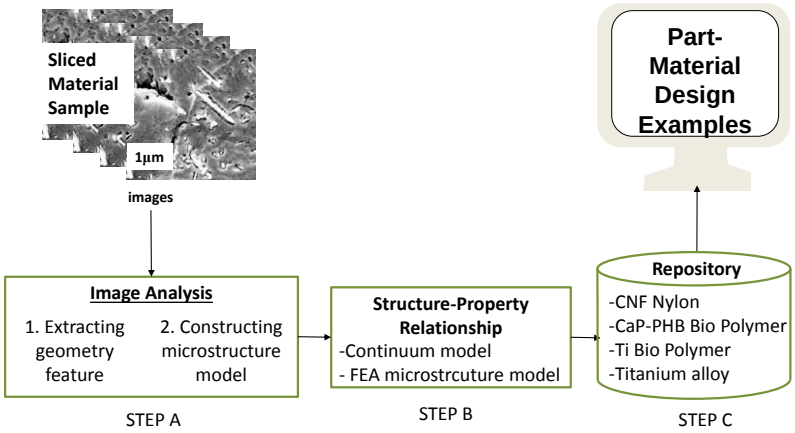

Figure 1 Proposed reverse engineering of material process

2 BACKGROUND

2.1 Heterogeneous Modeling

Heterogeneous materials are composed of different constituent materials. It displays continuously changing composition and/or microstructure. These materials have increasingly been used in engineering applications [2]. Current CAD systems have limited ability to model heterogeneous materials. Recently, several studies of heterogeneous material modeling systems have been explored. Kumar and Dutta [3] presented a set-based approach for spatial discretization of the solid interior by including variations in composition along with the geometry. Their implementation was restricted to polynomial functions. Kumar and Wood [4] proposed a finite element based method for modeling and optimizing material density distributions using particular design objectives and constraints. They proposed a method that used a four-node mesh and its associated interpolation functions. The method needed to be improved for describing arbitrary heterogeneous solids. In order to achieve heterogeneous modeling, some researchers used a mesh-free method, which does not rely on any form of spatial decomposition of the geometry. Wahlborg and Ganter [5] implemented an implicit approach to heterogeneous solid modeling (H-ISM). Their work used Boolean operators to construct heterogeneous models with both solid and material spaces. Pratap and Crawford [6] presented work that used existing research based on implicit procedural methods. They extended that work in order to build a tool to design volumetric material information. However, because these methods were focused on macro-structure, modeling and representing the microstructure of heterogeneous objects is beyond these studies.

2.2 Feature Extraction on Microstructure

Several researches have been proposed method of extracting geometry in the desired image. Leavers and Boyce [7] showed that a two-dimensional transform space could be used to encode the data associated with analytically defined shape primitives in the image space. They proposed that the form of the distributions in transform space associated with the shape primitives in image space may be deduced and used to derive convolution filters with which to locate those distributions. Leavers [8] used the Radon transform to decompose a binary edge image into its constituent shape primitives where those shape primitives are straight lines and arcs of conic sections. She proposed a technique that makes explicit certain geometric properties and spatial relations between the shape primitives which are then used to code for representation of shape.
Recently, Niezgoda and Kalidindi developed a size invariant Hough framework to detect arbitrary shapes [9]. They generalize the concept of a Hough filter by implementing other parameters of interest in the complex phase. The research focused on exploring the application of a phase-coded generalized Hough transform.

3 METHOD

3.1 Surfacelet Models

This chapter presents a brief overview of relevant method. A surfacelet model can be generated by a combination of Radon-like surfacelet and wavelet transforms as introduced in [10]. In this research, we consider a Radon, Radon-like transforms in the analysis. The Radon, Radon-like and wavelet transform will be summarized here.

3.1.1 Radon Transform

Generally, the Radon transform is based on a function of integrals over straight lines. It is also an integral transform whose inverse is used to reconstruct an image from medical CT scans [11]. The inverse Radon transform is used to reconstruct the original image from the sensor data obtained during the imaging step. Since the Radon transform is based on integrals over straight lines, if geometric features with linear geometry exist in the object to be imaged, those linear features can be recognized readily. This capability has been used in many applications in image compression [12], image reconstruction [13], and feature recognition [14].

The Radon transform is defined as the line integral along each line, *L*, in the XY plane:

$$R_f(L) = \int_L f(x)|dx| \quad (1)$$

or

$$R_f(\alpha, b) = \int_{-\infty}^{\infty} f\big((usin\alpha + bcos\alpha), (-ucos\alpha + bsin\alpha)\big)du \quad (2)$$

If a parametric model of a line is used:

$$p(u) = ((u\sin\alpha + b\cos\alpha), (-u\cos\alpha + b\sin\alpha)) \quad (3)$$

where *u* is the parameter along the line, α is the angle of the line, and *b* is its distance from the origin.

The Radon transform can be extended to three or higher dimensions. In three-dimensional cases, the linear geometry is a plane [13].

3.1.2 Wavelet Transform

In the domain of 2D shape representations, wavelets are among the most popular multi-resolution representations. Similar to Fourier analysis, wavelet analysis represents and approximates signals (or functions). However, instead of sinusoidal functions in Fourier analysis, the functional space for wavelet analysis is decomposed based on a scaling function *j(t)* and a wavelet function *y(t)* with the one-dimensional variable t for multi-resolution analysis. Wavelets are self-similar and can be scaled up and down. More specifically, the wavelet function

$$y_{\alpha,b}(t) = \alpha^{-1/2} y(\alpha^{-1}(t - b)) \quad (4)$$

is scaled by a scaling (dilation) factor *a* and translated by a translation factor *b*. Although certain forms (e.g. Haar, Daubechies, Morlet, etc.) have been used extensively, *y(t)* is actually general and can be customized for specific problems. The most important feature of wavelets is that they are localized in both real (time) and reciprocal (frequency) spaces due to the property of regularity and vanishing moments. In the geometric modeling domain, the wavelet transforms were used to describe planar curves with multiple resolutions [15].

3.1.3 Surfacelet Transform

The simplest surfacelet is the ridgelet transform, which is the 1D wavelet transform of the surface integral resulting from the Radon transform (Equation 2) as in Equation 5 [10]:

$$\text{2D: } \Psi_{b,\alpha} = \langle R_f(\alpha, b), y(\alpha, b))\rangle \quad (5a)$$

$$\text{3D: } \Psi_{b,\alpha,b} = \langle R_f(\alpha, b, b), y(\alpha, b, b))\rangle \quad (5b)$$

Equation 5 can be generalized for other types of surfacelets. The surfacelet transform can be rewritten as a general surfacelet basis function by modifying Equation 4 as

$$y_{\alpha,b,\boldsymbol{p}}(t) = \alpha^{-1/2} y(\alpha^{-1} r_{b,p}(r)) \quad (6)$$

where $\mathbf{r} = (x,y,z)$ is the location in the domain Ω in the Euclidean space, $y{:}R \rightarrow R$ is a wavelet function, $r_{b,p}$: $R^3 \rightarrow R$ is a surface function so that $\rho_{b,p}=(x,y,z)=0$ implicitly defines a surface, with the translation factor b and the shape parameter vector $p \in R^m$ determining the location and shape of surface singularities, respectively. For example, the 2D ridgelet is formed by introducing angular element $\alpha \in [0,\pi)$ into the wavelet function as

$$y_{a,b,\alpha}(r) = y_{a,b}(x\cos\alpha + y\sin\alpha) = a^{-1/2} y(a^{-1}(x\cos\alpha + y\sin\alpha - b)) \quad (7)$$

The 2D ridgelet is shown schematically in Figure 2a.
The 3D ridgelet represents plane singularities and is defined as

$$y_{a,b,\alpha,\beta}(r) = a^{-1/2} y(a^{-1}(\cos\beta\cos\alpha \cdot x + \cos\beta\sin\alpha \cdot y + \sin\beta \cdot z - b)) \quad (8)$$

where α is rotation about the Z axis, $\beta \in [0,\pi)$is a new angular parameter about the local X axis, and b is a translation along the local Y-axis, as shown in Figure 2b. Here the shape parameter vector is $\mathbf{p} = (\alpha,\beta)$. Similarly, a surfacelet that represents cylindrical singularities can be defined as

$$y_{a,b,c,\alpha,\beta,r_1,r_2}(r) = a^{-1/2} y\left(a^{-1}\left[\begin{matrix} r_1(\cos\beta\cos\alpha \cdot x + \cos\beta\sin\alpha \cdot y + \sin\beta \cdot z - b)^2 + \\ r_2(-\sin\alpha \cdot x + \cos\alpha \cdot y)^2 \end{matrix}\right]\right) \quad (9)$$

where parameters r_1 and r_2 describe the major and minor radii of the cylindrical shape.
The parameters of surfacelets can be geometrically interpreted as follows. For 3D ridgelets as in Figure 2b, any point on a plane $\cos b \cos\alpha \cdot x + \cos b \sin\alpha \cdot y + \sin b \cdot z = t$ has the same evaluation of the wavelet function $y(\alpha^{-1}(t-\beta))$. Therefore, the isosurfaces of Equation 8 are planes. The cylindrical surfacelet is shown in Figure 2c, where the isosurfaces of Equation 9 are seen as cylinders. The 2D version of cylinderlets is shown in Figure 2d.

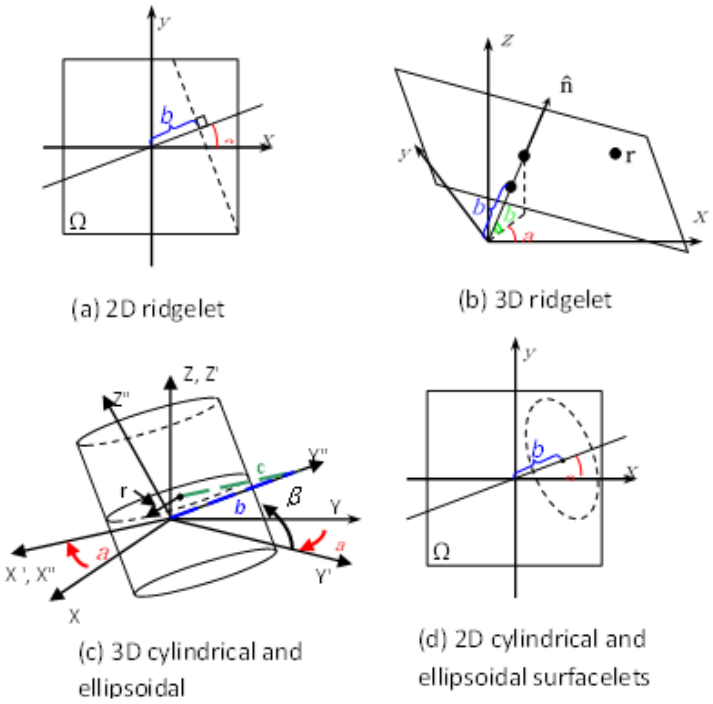

Figure 2. Geometric interpretation of Surfacelet

3.2 Feature Recognition Method for Microstructure Features

Materials with well-defined microstructure features, such as fibers or particles, can be recognized using surfacelet transforms. In order to represent a recognized feature, parameters are used. For example, linear feature like fibers can be characterized using their position, orientation, and sizes. In a 2D image, fibers can be recognized using 2D ridgelets, since the fibers are linear lines. 2D ridgelets provide orientation and location information directly. By analyzing results of the surfacelet transform, length of fiber can be obtained. Similarly, grain boundaries often have linear shapes and so can be recognized by 2D ridgelets in 2D images, and by 3D ridgelets if 3D voxel datasets are analyzed.

Microstructure features can be extracted using surfacelet representations, which are computed by first applying the Radon transform or a Radon-like transform to the image, to convert line or edge singularities to point singularities. Then, by applying a wavelet transform to the results of the Radon transform or a Radon-like transform, a representation of the image can be produced that is potentially sparse. The feature recognition method is presented in Figure 3, which is step A in Figure 1. Microstructure features can be found computationally from surfacelet representations. It is important to recognize that the results of applying the Radon, Radon-like, wavelet, or surfacelet transforms are coefficient sets. As a result, microstructure features can be recognized by finding peaks (observed as bright spots in renderings of these coefficient sets) in the Radon or Radon-like or wavelet transforms. Recognized microstructure features are used to construct a microstructure model. This model enables us to calculate the effective mechanical properties of microstructure. Finally, by doing that, we are able to achieve structure-property relationships of microstructure. These relationships can be integrated into current CAD system so that heterogeneous CAD system can be obtained.

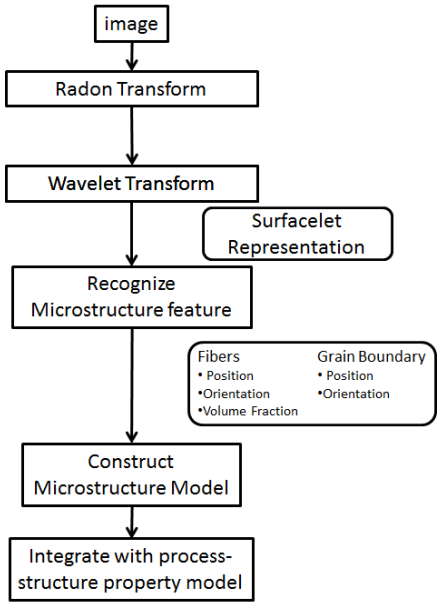

Figure 3. Microstructure feature recognition method

3.3 Feature extraction using a surfacelet method

2D linear feature extraction can be obtained computationally using the 2D Radon transform. The 2D Radon transform generates 2D coefficient sets. A single linear line can be represented as a couple of sinusoidal waves, shown in Figure 4. Those sinusoidal waves overlap at one point and the result resembles butterfly wings. Butterfly wings connect at the overlap point, which is the brightest point in the set of curves. The brightest point represents the maximum value in transform space, called a peak. Butterfly wing shape in the 2D coefficient set of the Radon transform is extended in the (α) direction as shown in Figure 4b. Depending on the image 2D coefficient sets can be complicated, which generate many peaks, as will be shown Section 4. By finding peaks in the Radon transform coefficient set, geometric feature information can be extracted. The challenge is that often a feature, such as a fibers or grain boundary, will be represented by several of these bright points close to one another in the Radon transformed parameter space. This type of representation will be called over-representing features. This is often observed with long fibers or grain boundaries; two or three neighboring angles (α, β) will have large transform values. Conversely, a single peak in the Radon transform may correspond to more than one microstructure feature; for example, if two fibers were collinear and were represented by a single peak, this feature would be called under-represented features. A simple 2D example of an over and under-represented feature is shown in Figure 5. In order to solve these issues, this work will apply three techniques to the Radon transform.

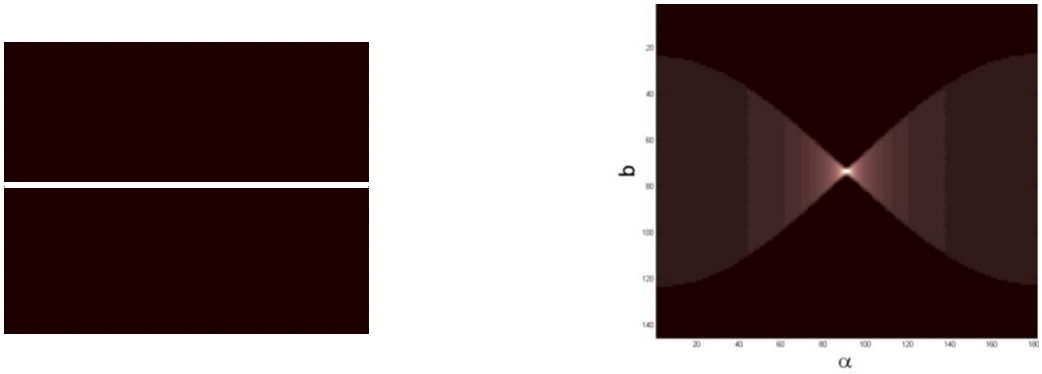

(a) Single linear feature (b) Shape of butterfly wing of linear feature

Figure 4. Single linear feature and its shape of butterfly wings

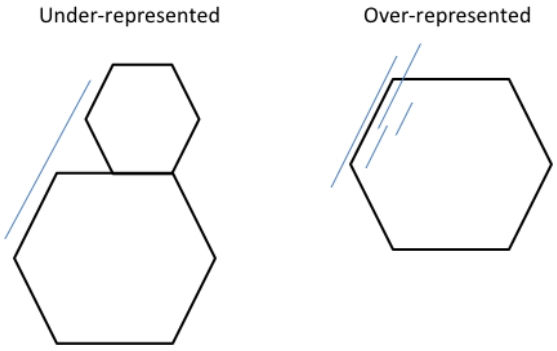

Figure 5. Simple example of an over and under-represented feature

The first technique is masking. Masking allows us to identify peaks, which correspond to linear features in the image. Equation (10) is a 3 x 3 convolution mask of the form.

$$\begin{pmatrix} 0 & -2 & 0 \\ 1 & 2 & 1 \\ 0 & -2 & 0 \end{pmatrix} \qquad (10)$$

Equation (10) emphasizes the peak by multiplying 2 to the peak value. On the other hand, the pixels above and below the peak point will be de-emphasized by multiplying by -2. The matrix dimension can be expanded depending on the size of the transform coefficient matrix, or it can be rotated depending on the shape of the butterfly wing. By using this mask, peaks in transform space can be found and over-representation can be avoided.

The second technique is to analyze the high frequency component of the wavelet transform to find microstructure features. In surfacelet transforms, a Radon transform and a wavelet transform are applied to the microstructure image. The wavelet transform contains both low and high frequency coefficients, which represent respectively low and high resolution information about the image. The high resolution component contains abundant information to extract linear features, and it emphasizes large gradients in the image. These emphasized gradients help to extract information to represent linear geometry. Two factors, point singularities and large gradient, hold promise for recognizing peaks.

Once we apply either masking or high frequency component of the wavelet transform, we use a clustering technique to select peak values among complicated results. If the image contains complicated geometric features, the result of the Radon or wavelet transform can become very complicated, with numerous butterfly wings rotated and overlapped. It is difficult to find linear features by detecting all peak values. Over-represented and under-represented features are common occurrences in this case. Peak values close to one another in the Radon transform will be clustered together using a k-means clustering method based on pair-wise distances between peaks. Among the peak values in the cluster, we take the largest value in the clustering area. By using clustering for the complicated result, the peaks of the linear features can be chosen.

3.4 Linear feature angles

Determining the angle of the linear geometric feature is illustrated with a simple example of a fiber–reinforced composite material. Figure 6a shows the sample microstructure, with vertical and horizontal fibers spaced 100 μm apart. The surfacelet transform is applied to the sample's image. The Radon transform of the microstructure results in four sets of non-zero coefficients, as four bright spots shown in Figure 6b, which illustrates the efficiency of surfacelet representation for microstructures with linear elements. Angles of the four fibers from Figure 6a are identified by coefficients of (α, b) = (0,50), (0,150), (90,50), and (90,150). The α values correspond to the angles of 0 and 90 degrees, while the b values correspond to the positions of the fibers. Using the Radon transform, it is possible to recognize angle of the fibers in the image.

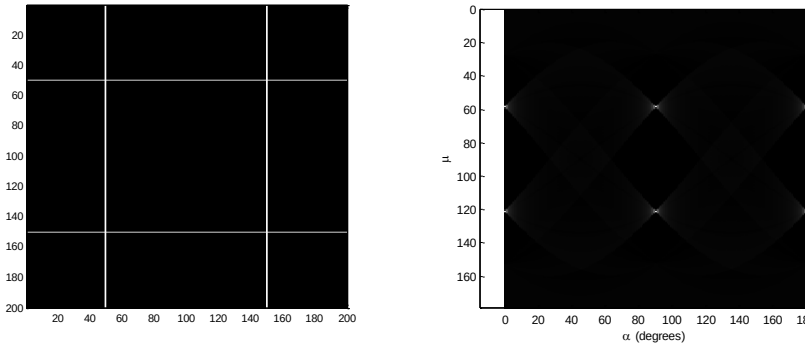

a. Fiber-reinforced composite microstructure **b. Radon transform**

Figure 6. Simple synthetic fiber-reinforced microstructure and surfacelet representations

3.5 Linear feature length and position

Consider the linear microstructure feature shown in Figure 7. By analyzing the butterfly wing geometry around a peak, the length and position of a linear feature can be computed. The Radon transform of the linear feature can be illustrated using Figure 7, where θ is the angle of the linear feature (which is α + 90 degrees), and the linear feature is represented by the perpendicular line to the linear feature at a distance, b, from the origin and its angle, α. P_0 represents the foot of the perpendicular from the origin to the linear geometric feature. If we take the maximum Δα value, the Radon transform would give two displacement values, $b_{u1}$and b_{u2}, which are the foot of the perpendicular from the origin to the lines 1 and 2 that pass through the linear feature end points, Q and R. As shown in Figure 7, the cross points of the line 1, 2 and the linear feature make a right triangle (ΔQRS). Two displacement values, $b_{u1}$and $b_{u2,}$ are represented in the Radon transform coefficient set, as shown in Figure 8a. The height of the triangle can be expressed as equation (11).

$$\overline{QS} = b_{u1} - b_{u2} \tag{11}$$

By using Δ α and height of a right triangle, length of the linear segment can be calculated.

$$length = \overline{QR} = \overline{QS} * \sin(\Delta\alpha) \tag{12}$$

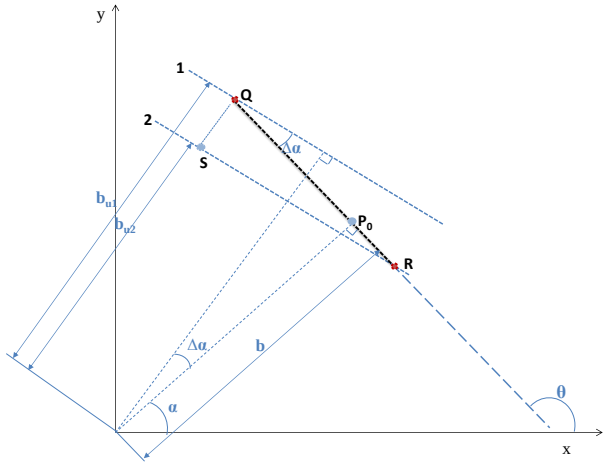

Figure 7. Schematic of linear feature of characterization

Based on the research conducted by Leaver and Boyce [7] the position of line segment along its angle θ, can be determined. The length of the contributing point from the foot of the perpendicular, p_0, is as follows:

$$p = tan(\psi) \tag{13}$$

where $tan(\psi)$ is the slope of a bounding curve of the butterfly wing as shown in Figure 8b. Therefore, we obtain the lengths of the linear lines $\overline{QP_0}$ and $\overline{P_0R}$

$$p_1 = \overline{QP_0} = tan(\psi_1),\ p_2 = \overline{P_0R} = tan(\psi_2) \tag{14}$$

Having found p_1 and p_2, the linear feature length can be computed as the sum of these quantities:

$$Length = p_1 + p_2 \tag{15}$$

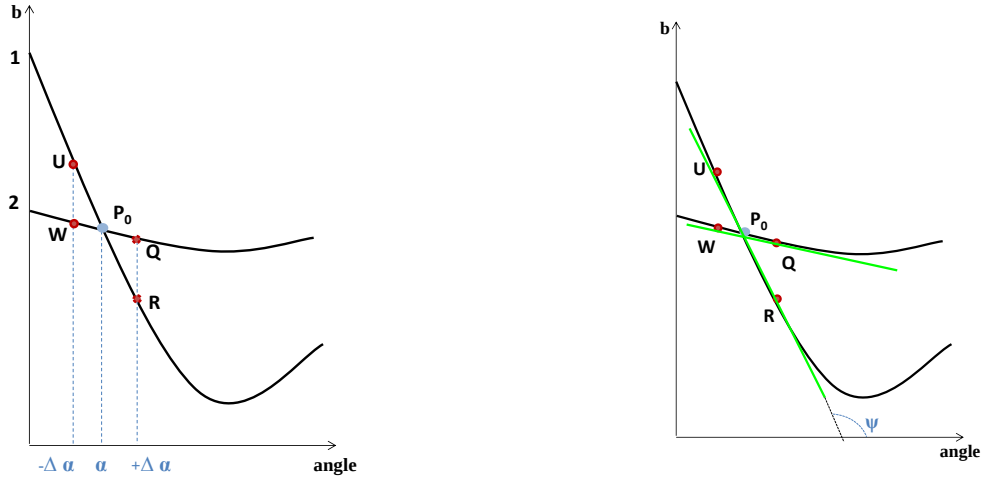

(a) Cross points of butterfly wings (b) slope of butterfly wings

Figure 8. The Radon transforms butterfly wings

4 EXAMPLES

4.1 Calcium-Phosphate fiber

In order to demonstrate our proposed method, we use a synthetic nanocomposite with 5 weight-percent fibers. The nanocomposite is based on a nanofiber-filled biodegradable polymer, polyhydroxybutyrate (PHB), with calcium-phosphate (CaP) nanofibers [16]. We use a synthetic microstructure, since we can directly control fiber length, position, and orientation in order to compare with the feature recognition results. Assuming that fibers are randomly distributed, a sample microstructure that consists of nine fibers is shown in Figure 9.

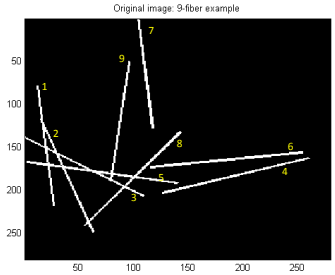

Figure 9. Calcium-Phosphate Fibers

The surfacelet methods with masking, high frequency component on wavelet and clustering were investigated to recognize microstructure of Figure 9. These methods enable users to select peaks corresponding to fibers. All fibers were recognized at the red circle in Figure 10a using the regular surfacelet based method, at the bright convergence spot in Figure 10b using masking, and at the white circle in Figure 10c using the high frequency component on the wavelet. Each indicated spot corresponds to the fiber angle and location. In order to choose the correct peak point, we used clustering.

Table 1 shows the results from each method that finds peak in the Radon transform coefficient matrix. Result from combination with the Radon transform and masking, combination with the Radon transform and high frequency component in wavelets are shown. The results give almost same result as is obtained by using regular Radon transform.

We are able to calculate the length and position of the fibers using these angles shown in Table 1. Since we have peak values, we can find each of the butterfly wings, we call cross point of butterfly wing. Cross points of butterfly wings are taken at angles $\Delta\alpha$ on each side of the peak value. Cross points of the butterfly wings can be found as shown in Figure 11. For example, each of the 4 white spots corresponds to U, W, Q, and R in Figure 8b.

By using the cross point of the butterfly wing, we obtain the length of the fibers and their positions. Figure 12 shows an image of the reconstructed fibers. Even though line 7 is located lower than its actual location, the fibers are located at actual fiber location. All fiber lengths and angles are almost the same as actual fibers. Table 2 shows the error between the actual and the reconstructed fibers. Table 2 shows the error between the actual and the reconstructed fibers. Note that length 1 is obtained by using the first length calculation method, given in Equation 12, while length 2 is obtained by the method given in Equation 16. These two means calculated the length give almost same result. Since masking and the high frequency component of the wavelets produce similar peak values, their reconstructed images are the same.

Table 1. Peak values from different feature recognition methods

fiber	Regular radon transform with clustering	Radon + masking with clustering	Radon + high frequency comp with clustering
1	7	7	8
2	21	21	21
3	59	59	60
4	108	107	107
5	81	80	80
6	98	98	98
7	7	9	6
8	142	142	142
9	174	174	174

Table 2 Error between actual fiber and reconstructed fiber

Fiber	length 1	length 2	angle %
	Height * sin(Δφ)	P1 + P2	
	Length error (%)	Length error %)	
1	15.53	15. 4	0.69
2	9.54	9.65	0.80
3	3.39	3.26	0.81
4	22.22	22.31	0.50
5	2.51	2.38	0.27
6	1.68	1.80	0.55
7	8.70	8.82	1.10
8	9.81	9.93	0.65
9	6.65	6.77	0.63

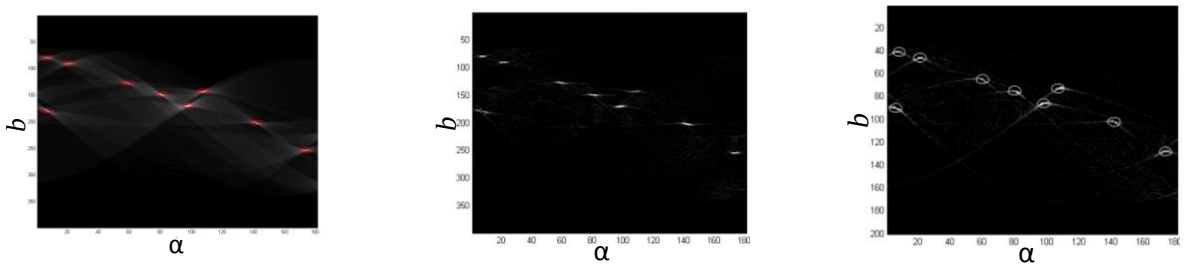

(a) Regular Radon transform (b) Radon transform + Masking (c) Radon transform + High frequency component in wavelets

Figure 10. Result of the Radon transform with different feature recognition methods

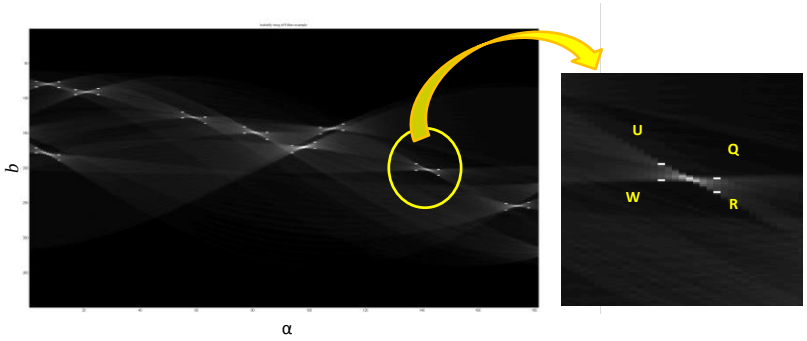

Figure 11. Result of the Radon transform with cross points of the butterfly wings for 9-fiber example

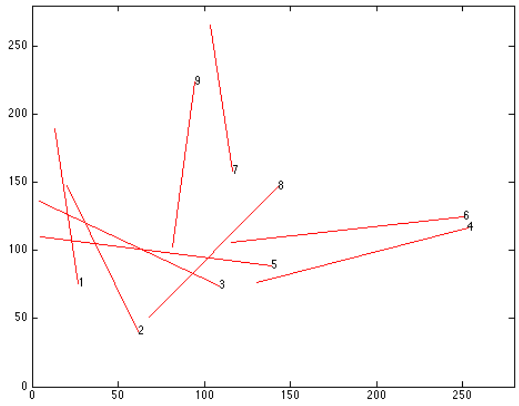

Figure 12. Reconstructed image of 9-fiber example

4.2 Metal alloy

As a second example, 2D ridgelet transformations will be applied to a dataset obtained from a 10x10x10 µm IN100 nickel-base super-alloy sample [17], shown in Figure 13. Grain boundaries will be recognized in part of the smoothed 2D image.

Part of one cross section through the dataset was smoothed manually, since the original dataset was too coarse (only 41x41 pixels) and was used for this example. Figure 14 shows part of the smoothed cross-section. By using the proposed method, angles of linear feature were recognized. Three different variations of surfacelet based methods were performed which are regular Radon transform with clustering, the Radon transform with masking and clustering, and the Radon transform with high frequency component of wavelet and clustering. Among three

variations, high frequency component of wavelet produces the most promising result. As shown in Table 3, most of linear features were detected by the high frequency component of wavelet. By using detected angles, the cross points of the butterfly wings in the 2D coefficient set were found, as shown in Figure 15. By using these cross points, we obtain the position, length, and angle of the grain boundary segments shown in Figure 14. The reconstructed line segments from this cross section are shown in Figure 16. However, in order to construct grain boundaries, line segments need to be connected. If the end points of the line segments were close to one another, they were assumed to represent shared vertices and were connected, with the positions of the shared vertices computed by averaging all shared cross point positions. The reconstructed grain boundary image is shown in Figure 17.

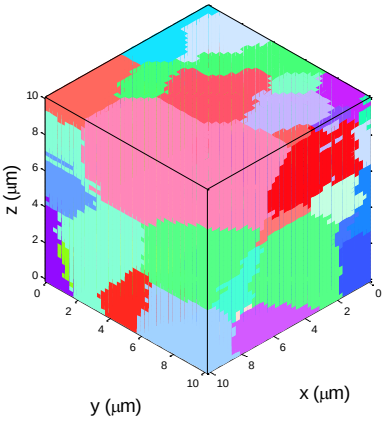

Figure 13. IN100 voxel dataset

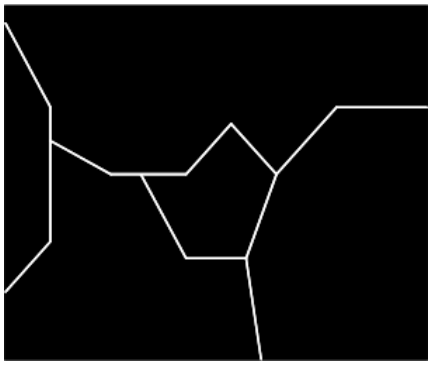

Figure 14. Cross section of part of IN100 example

Table 3. Peak values from different feature recognition methods for alloy example

line segment	Regular radon		Radon + masking		Radon + high freq. comp.	
	disp.	angle	disp.	angle	disp.	angle
1	95	1	94	2	98	1
2	258	19	258	19	260	19
3	170	63	171	62	172	63
4	159	91	159	91	162	89
5	180	149	180	150	182	150
6	269	181	269	180	270	180
7	153	56	None		152	55
8	170	107	None		174	108
9	None		120	131	122	131
10	None		None		216	143
11	None		None		130	172
12	None		None		234	91
13	159	84	None		None	
14	None		140	91	None	

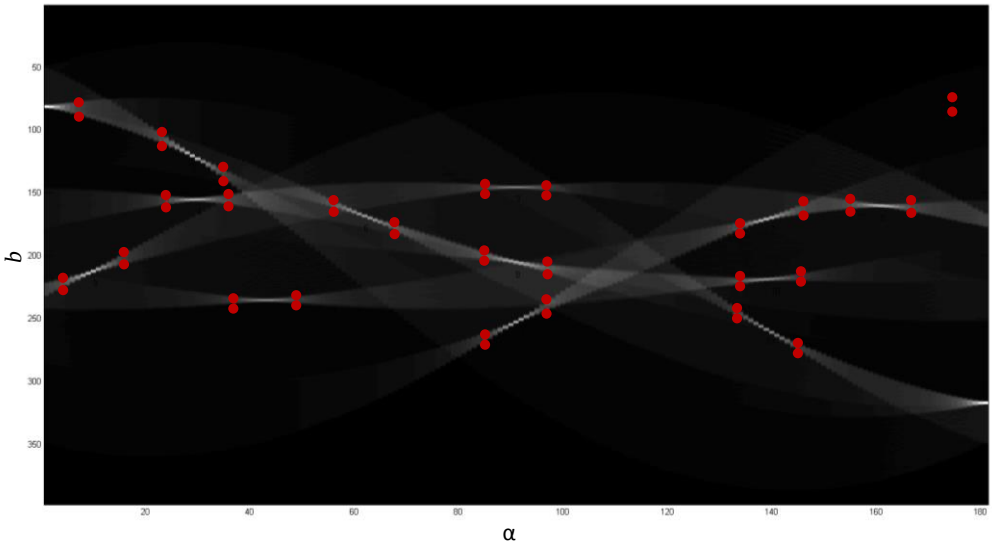

Figure 15. Result of the Radon transform with cross points of the butterfly wings for IN 100 example

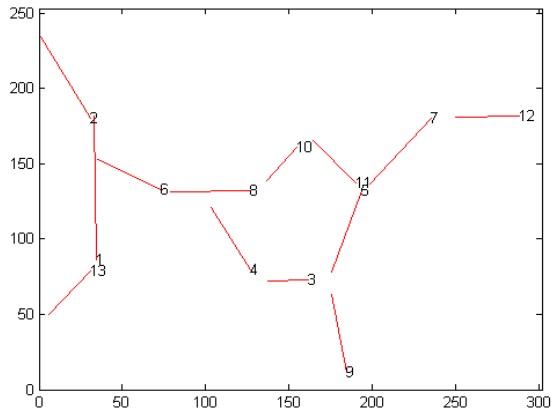

Figure 16. Reconstructed image of line segment for cross section of IN 100 example

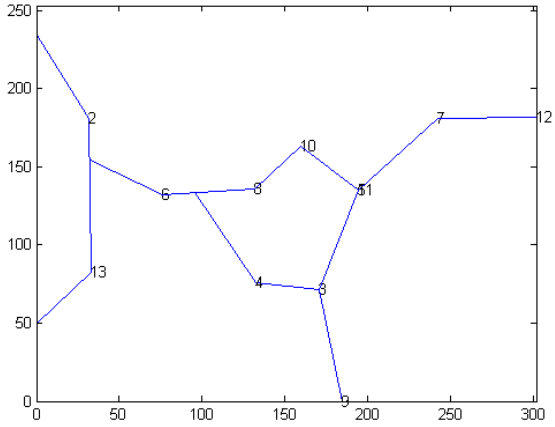

Figure 17. Reconstructed grain boundaries of IN 100 example

4.3 Copper specimen fabricated by EBM

In order to apply our method to real grain boundaries produced by an AM process, we used a copper microstructure image. Figure 18 shows a surface of EBM fabricated Cu specimen containing Cu_2O precipitates [18]. Since the image includes noise, the 2D coefficient set of the Radon transform is complicated. From the coefficient set, we select peak values, which represent the angle of linear features. Then, the cross points of the peak values are found with appropriate threshold, shown in Figure 19. A reconstruction image of linear features is shown in Figure 20. By using the reconstructed linear features, we construct grains, shown in Figure 21. A reasonably good match was achieved by recognizing grain boundaries and reconstructing grains, as can be seen in Figure 21b.

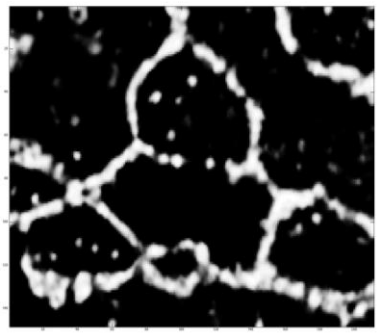

Figure 18. Copper specimen fabricated by BEM

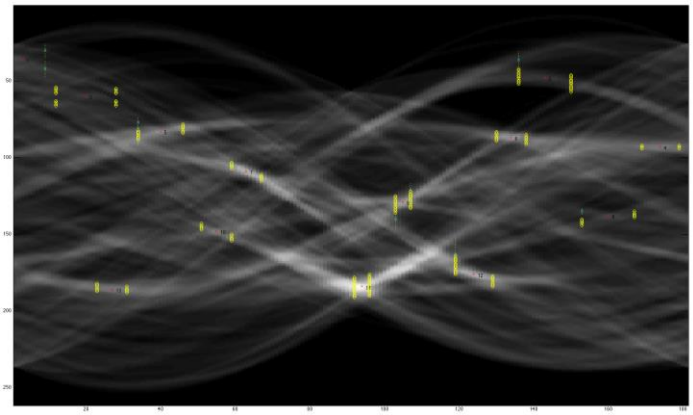

Figure 19. Result of the Radon transform with cross points of the butterfly wings for Copper example

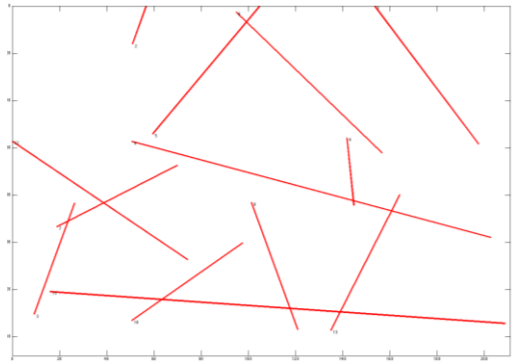

Figure 20. Reconstructed linear feature of Copper example

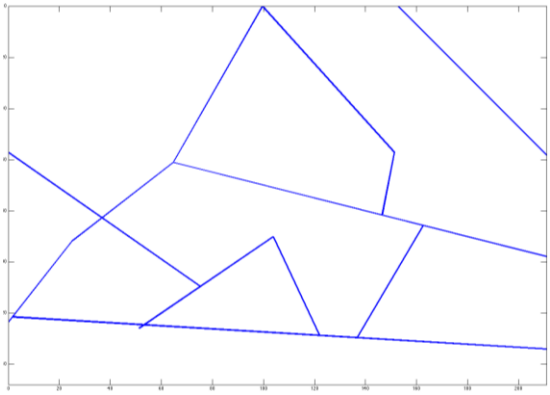

(a) Reconstructed grain boundaries

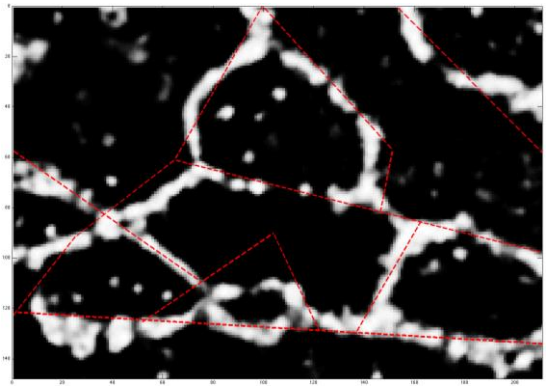

(b) Reconstructed grain boundaries overlapped with input image

Figure 21. Reconstructed image of Copper example

5 CONCLUSION

A new approach for reverse engineering of materials was presented that seeks to construct material microstructure models. The approach recognizes microstructure features from 2D images of material cross-sections. Linear features, such as fibers and grain boundaries, can be recognized by applying Radon and surfacelet transforms. From this study, it can be concluded that linear features can be recognized readily. Fibers in 2D images can be recognized as lines

using the 2D ridgelet transform. Grain boundaries in metal alloys are also recognized as lines. In addition, a real image including noise also can be recognized as lines using the proposed method. Linear features are recognized by three different methods, 1) Radon transform, 2) Radon transform with masking, 3) Radon transform with high frequency component of the wavelet transform. In order to choose peak value from each method, we cluster peaks, and select the highest peak in each cluster. Therefore, selected peaks provide angles of linear features and sets of 2D coefficients of the Radon transform enable to obtain estimated length and position of the linear feature. Three examples, PHB fiber, metal alloy, and copper, are used to demonstrate this. Among the three methods, high frequency component of wavelet produces the most promising result. In addition, the calculated lengths and positions of linear features were reasonably close to those from the original image.

The feature recognition method using Radon and surfacelet transform works well with linear features. Angles of the linear features are recognized accurately, while length and position are extracted with small errors. This is because the length and position calculation of linear features highly depends on accurately identifying the cross points of the butterfly wings in the Radon transform. In addition, the limited resolution of Radon transforms causes the points U, W, Q, and R to be identified with significant error in some cases.

Further work will investigate additional types of surfacelet transforms for recognizing various other microstructural features, including ellipsoidal shapes and more complex grain boundaries. Additionally, integration of microstructure models with CAD systems will be demonstrated, enabling heterogeneous modeling of CAD models. In addition to geometry, material information, including compositions, microstructures, and properties, is needed. With this information, structure-property relationships can be modeled such that effective mechanical properties at larger size scales can be computed from material property information at small scales.

ACKNOWLEDGMENTS

The authors gratefully acknowledge support from the National Science Foundation, grant CMMI-1030385. Any opinions, findings, and conclusions or recommendations expressed in this publication are those of the authors and do not necessarily reflect the views of the National Science Foundation

REFERENCE

1. Rosen, D.W., N. Jeong, and Y. Wang. *A Hierarchical, Heterogeneous Material CAD Model with Application to Laser Sintering*. in *Solid Freeform Fabrication Symposium*. 2010.
2. Torquato, S., *Random heterogeneous materials: microstructure and macroscopic properties*. Vol. 16. 2001: Springer.
3. Kumar, V., D. Burns, D. Dutta, and C. Hoffmann, *A framework for object modeling.* Computer-Aided Design, 1999. **31**(9): p. 541-556.
4. Kumar, A.V. and A. Wood. *Representation and design of heterogeneous components*. in *Proceedings of SFF Conference, Austin, Texas*. 1999.
5. Wahlborg, J., M.A. Ganter, D.T. Schwartz, and D. Storti. *H-ISM: An Implementation of Heterogeneous Implicit Solid Modeling*. 2002. ASME.
6. Pratap, A. and R.H. Crawford, *Implementation of a functionally gradient material modeling and design system*. 2003, University of Texas at Austin.

7. Leavers, V. and J. Boyce, *The Radon transform and its application to shape parametrization in machine vision.* Image and Vision Computing, 1987. **5**(2): p. 161-166.
8. Leavers, V., *Use of the Radon transform as a method of extracting information about shape in two dimensions.* Image and vision computing, 1992. **10**(2): p. 99-107.
9. Niezgoda, S.R., S.R. Kalidindi, X. Hu, G.A. Cingara, D.S. Wilkinson, M. Jain, P. Wu, R.K. Mishra, M. Arafin, and J. Szpunar, *Applications of the Phase-Coded Generalized Hough Transform to Feature Detection, Analysis, and Segmentation of Digital Microstructures.* Computers, Materials, & Continua, 2010. **14**(2): p. 79-98.
10. Wang, Y. and D.W. Rosen, *Multiscale Heterogeneous Modeling with Surfacelets.* Computer-Aided Design & Applications, 2010. **7**(5): p. 759-776.
11. Kak, A.C. and M. Slaney, *Principles of computerized tomographic imaging*. Vol. 120. 2001: Siam Philadelphia:.
12. Do, M.N. and M. Vetterli, *The finite ridgelet transform for image representation.* Image Processing, IEEE Transactions on, 2003. **12**(1): p. 16-28.
13. Lanzavecchia, S., P.L. Bellon, and M. Radermacher, *Fast and accurate three-dimensional reconstruction from projections with random orientations via radon transforms.* Journal of structural biology, 1999. **128**(2): p. 152-164.
14. Jiang, X., W. Zeng, P. Scott, J. Ma, and L. Blunt, *Linear feature extraction based on complex ridgelet transform.* Wear, 2008. **264**(5): p. 428-433.
15. Daubechies, I., O. Runborg, and W. Sweldens, *Normal multiresolution approximation of curves.* Constructive Approximation, 2004. **20**(3): p. 399-463.
16. Kaur, J., *Properties of biologically relevant nanocomposites: effects of calcium phosphate nanoparticle attributes and biodegradable polymer morphology.* 2010.
17. Shenoy, M., Y. Tjiptowidjojo, and D. McDowell, *Microstructure-sensitive modeling of polycrystalline IN 100.* International Journal of Plasticity, 2008. **24**(10): p. 1694-1730.
18. Murr, L.E., S.M. Gaytan, D.A. Ramirez, E. Martinez, J.L. Martinez, D.H. Hernandez, B.I. Machado, F. Medina, and R.B. Wicker, *Microstructure architecture development in metals and alloys by additive manufacturing using electron beam melting*, in *2010 Solid Freeform Fabrication Symposium*. 2010: Austin, TX, USA. p. 308-323.